

# Quantized Ostwald Ripening of Colloidal Nanoparticles

Pinar Dagtepe and Viktor Chikan\*

Kansas State University, Department of Chemistry, 213 CBC Building, Manhattan Kansas 66506-3701

Received: June 2, 2010; Revised Manuscript Received: August 4, 2010

Controlling the growth of nanoparticles (NP) in nanotechnology is crucial to produce high-quality particles with narrow size distribution. This simulation investigates the growth of colloidal semiconductor NPs in the presence of two distinctly sized NPs in the so-called “bimodal growth regime”. One of the sizes of the NPs is selected such that its radius falls below or close to the critical dissolution radius. These particles will act as sacrificial materials for a larger second size for the growth and size focusing. The bimodal distribution (or quantized Ostwald ripening) technique is found to be a slower process compared to the commonly used repeated injection technique to focus the size distribution of NPs. The slow growth condition could lead to a better reaction control over the NP synthesis. Slower growth will reduce the effect of inhomogeneous mixing in a scaled up production of NPs. The low monomer oversaturation over the growth could improve the overall quality of the NPs. The results presented here on colloidal NPs are potentially applicable to the size evolution of NPs on surfaces as well.

## Introduction

Controlling the growth of nanoparticles (NPs) is important in order to create uniform particles with narrow size distributions for both fundamental science and technology. Ostwald ripening (coarsening) is one of the general growth mechanism that controls NP syntheses.<sup>1–3</sup> In general, colloidal particles are inclined to minimize their surface-to-volume ratio, thereby their surface free energy. Lifshitz–Slyozov–Wagner (LSW) theory describes the size evolution of particles in terms of reducing the overall surface energy of the system. The LSW ripening critically depends on the solubility of the particles as a function of size.<sup>3</sup> In a system where small particles are in equilibrium with larger particles, the overall size and size distribution will increase over time.

A NP with radius larger (smaller) than a critical radius grows (dissolves), which is commonly called the Ostwald ripening. The critical radius is a function of the solution and NP's properties. The corresponding equation of the critical radius is as follows:<sup>4</sup>

$$r_{\text{cr}} = \frac{2\gamma V_m}{RT \ln S} \quad (1)$$

In this equation,  $S$  is supersaturation of the monomers in solution, which is the ratio of the actual monomer concentration to the monomer solubility over a flat surface;  $R$  is the gas constant;  $T$  is the temperature;  $\gamma$  is the specific surface energy; and  $V_m$  is monomer volume. The dissolution of small particles and growth of larger particles is explained by the curvature dependence of the chemical potential:<sup>5</sup>

$$\mu = \mu_0 + V_m \gamma \kappa \quad (2)$$

Here  $\mu_0$  is the chemical potential of atom on a flat interface,  $\kappa$  is mean interfacial curvature,  $V_m$  is molar volume, and  $\gamma$

represents specific surface energy. This equation points out the direction of material flow, from high to low curvature. Therefore, regions of high curvature (smaller particles) with high energy disappear and lower energy regions of larger particles prevail. As a result of the material flux, the total free energy of the system decreases. Ostwald ripening process results in broadening of the size distribution of NPs due to the consumption of small particles in order to assist the growth of larger ones with lower surface energy.<sup>6,7</sup> Simulation of the size evolution of NPs based on the LSW theory shows that the initial Gaussian size distribution of NPs will become asymmetric.<sup>8,9</sup>

The inverse process of the Ostwald ripening is the size focusing of NPs. Experimentally, several research groups have achieved narrowing of size distribution (focusing) in colloidal systems and NPs.<sup>7,10–16</sup> The simplest way to obtain size focusing is to utilize particles from longer reaction times and perform size selective separation based on the solubility difference of different sized particles.<sup>12,17</sup> The size selective precipitation method usually requires large amounts of solvent that could make the approach rather costly. Alternatively, NPs can be focused by fine-tuning the reaction conditions to achieve a supersaturated environment with respect to the monomer. At the practical level, this is carried out by using the so-called multiple-injection method. In the multiple injection method, when the size of the particles defocuses from a regular nanoparticle synthesis, a second injection of molecular precursors takes place. The second injection causes the broad distribution to refocus.<sup>7</sup> The multiple injection method requires precise timing, since the growth of the nanoparticles is rather fast at high temperatures. In addition, renucleation can take place from the relatively high monomer concentrations and solution inhomogeneities. Therefore, developing methods to increase the time to generate the size focusing is of key importance in industrial-scale laboratory synthesis of semiconductor nanocrystals with uniform size and shape.

The growth of NPs in the bimodal growth regime, which is studied by several groups,<sup>6,18–22</sup> has already been shown to result in narrowing of size distribution of NP systems. Peng's work<sup>22</sup> has revealed that focusing of size distribution takes place when

\* To whom correspondence should be addressed. E-mail: chikan@ksu.edu.

two different sized CdS NPs are mixed at higher temperatures. During the CdS ripening, the initial two different-sized particles possessing broad size distributions undergo size focusing. According to Peng, focusing of size distribution is observed due to the dissolution of small particles in CdS solution while larger particles do not dissolve.<sup>22</sup> This study demonstrates the effect of interparticle interaction on the size distribution for a diffusion-controlled process. A similar observation has been reported on CdSe nanoparticles. The bimodal distributions of CdSe NPs are formed spontaneously in the growth solution at low temperatures.<sup>20</sup> In this system, CdSe NPs with different size values coexist for hours, and focusing of size distribution takes place in the reaction system similarly to Peng's observation.<sup>20</sup> Another recent deliberate attempt to utilize bimodal distribution to focus the size distribution is presented by Fu et al. This group has applied the bimodal size distribution approach to ZnO NPs via "supersaturation control" of the monomers.<sup>21</sup> Besides solution-based nanomaterials, there are studies on the size evolution of nanomaterials on surfaces. One of the studies is on the island of nanostructured clusters. Ross et al.<sup>23</sup> have observed the narrowing of the size distribution of Ge islands upon a shape transition from pyramid to dome.

The motivation of this work is to examine how the addition of small sized sacrificial nanoparticles (SNPs) to the growth solution will affect the size focusing via Ostwald ripening. The results from the simulation aim to find optimum conditions to produce size focusing. In this numerical simulation, the growth rate of nanoparticles is calculated on the basis of a method under diffusion control.<sup>4</sup> The multiple injection method and the Ostwald ripening process are also considered to assess the usefulness of this approach. The effect of renucleation rate is also studied and the calculations show that bimodal distribution yields lower the rate of renucleation compared to the multiple injection method.

## Simulation Method

The numerical simulation method is used here to explain the behavior of bimodal size distribution of nanoparticles based on a literature method.<sup>4</sup> Growth of particles is controlled by the size-dependent growth rate (eq 3a).<sup>4</sup>

$$\frac{dr^*}{d\tau} = \frac{S - e^{1/r^*}}{r^* + K e^{\alpha/r^*}} \quad (3a)$$

$$r^* = \frac{RT}{2\gamma V_m} r \quad (3b)$$

$$\tau = \frac{R^2 T^2 D C_{\text{flat}}^0}{2\gamma^2 V_m} t \quad (3c)$$

$$K = \frac{RT}{2\gamma V_m k_g^{\text{flat}}} \frac{D}{C_{\text{flat}}^0} \quad (3d)$$

In these equations, dimensionless radius, time, and  $K$  are used given by eqs 3b and 3c, respectively.  $S$  is the supersaturation of the monomers in solution,  $T$  is the temperature,  $R$  is the gas constant,  $\alpha$  is the transfer coefficient with a value of 0.5,  $D$  is diffusion coefficient,  $C_{\text{flat}}^0$  is solubility of the monomer in equilibrium with a flat surface,  $k_g^{\text{flat}}$  is the rate constant for a first-order deposition reaction, and  $K$  is the ratio of the diffusion

**TABLE 1: Parameters and the Values Used in the Simulation<sup>a</sup>**

parameter	value
temperature	573 K
monomer volume ( $V_m$ )	$3.29 \times 10^{-5} \text{ m}^3/\text{mol}$
simulated volume	$3 \times 10^{-18} \text{ m}^3$
$K$ parameter describing the type of control	0.001
transfer coefficient ( $\alpha$ )	0.5
monomer solubility	$10^{-2} \text{ mol/m}^3$
specific surface energy ( $\gamma$ )	0.125 J/m <sup>2</sup>

<sup>a</sup> Taken from ref.<sup>4</sup>

**TABLE 2: Different Trials of the Simulation**

simulation	no. of monomers		sizes of nanoparticles (nm)	
	SNP	larger size	SNP	larger size
1	$8 \times 10^4$	$2 \times 10^3$	1	3.5
2	$4 \times 10^4$	$2 \times 10^3$	1	3.5
3	$2 \times 10^4$	$2 \times 10^3$	1	3.5
4	$8 \times 10^4$	$2 \times 10^3$	1	3
5	$8 \times 10^4$	$2 \times 10^3$	1	4
6	$8 \times 10^4$	$2 \times 10^3$	1	4.5
7	$8 \times 10^4$	$5 \times 10^2$	1	3.5
8	$8 \times 10^4$	$1 \times 10^3$	1	3.5
9	$8 \times 10^4$	$1.5 \times 10^3$	1	3.5
10	$8 \times 10^4$	$2 \times 10^3$	1	3.5
11	$8 \times 10^4$	$3 \times 10^3$	1	3.5
12	$8 \times 10^4$	$4 \times 10^3$	1	3.5
13	$8 \times 10^4$	$8 \times 10^3$	1	3.5
14	0	$2 \times 10^3$	1	3.5
15	$2 \times 10^4$	$2 \times 10^3$	1	3.5
16	$3 \times 10^4$	$2 \times 10^3$	1	3.5
17	$4 \times 10^4$	$2 \times 10^3$	1	3.5
18	$5 \times 10^4$	$2 \times 10^3$	1	3.5
19	$6 \times 10^4$	$2 \times 10^3$	1	3.5
20	$8 \times 10^4$	$2 \times 10^3$	1	3.5
21	$1.2 \times 10^5$	$2 \times 10^3$	1	3.5
22	$1.6 \times 10^5$	$2 \times 10^3$	1	3.5

constant of the monomer to the reaction rate constants and indicates whether it is diffusion ( $K \ll 1$ ) or the reaction-controlled ( $K \gg 1$ ) process. It has been shown that the diffusion controlled reaction is the one that produces size focusing; therefore, in this system a value of 0.001 for  $K$  is used. This also implies that solvation effects are not rate-limiting steps under these conditions. The volume of the solution simulated is  $3 \times 10^{-18} \text{ m}^3$ . The parameters used in the calculations are given in Table 1 and are derived from the material parameters of CdSe nanoparticles synthesis. The simulation is carried out on the basis of the above equations and the equations are implemented in a MATLAB program.

This simulation focuses on the effect of SNP (sacrificial nanoparticle) to the growth solution (quantized Ostwald ripening-QOR) in comparisons with the Ostwald ripening (OR) process and the multiple injection method (MI). In the QOR approach, 1-nm-sized CdSe nanocrystals are added to the particles sizes changing between 3 and 4.5 nm with 10% size distribution. The large difference in nanoparticles sizes is necessary to reduce mixing between the two distinct sizes during the evolution of the growth solution. The 10% deviation from the average size corresponds to the experimentally achievable size distributions.<sup>24</sup> The number of SNPs used is between  $5 \times 10^2$  and  $8 \times 10^4$  and the larger size ranges from  $5 \times 10^2$  to  $1.5 \times 10^5$  (a full list of number of particles and sizes used in the simulation is given in Table 2) in the simulated volume. In the multiple injection (MI), instead of addition of small particles, the corresponding number of monomers is calculated and added

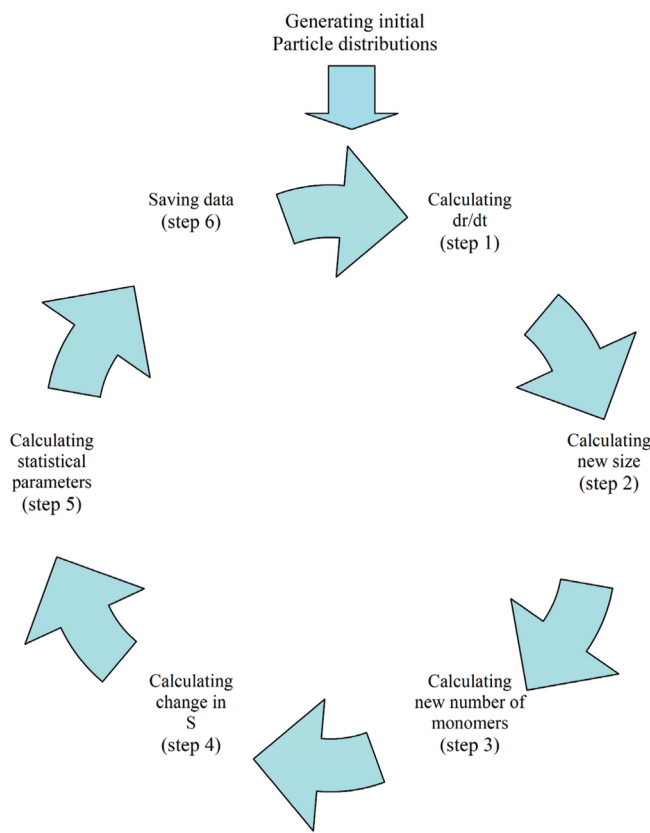


**Figure 1.** Flowchart of the steps of the simulation.

to the growth solution as it is carried out in the experimental multiple injection method (one-time injection of molecular precursors is considered in the simulation which takes place at  $t = 0$ ).<sup>4,7</sup> This step ensures that direct comparison of the growth kinetics can be made, because the number of monomers in the solution (free monomers and monomers bond to the NPs) are the same in both the QOR and MI approach.

$$S = \exp\left[\frac{2\gamma V_m}{rRT}\right] \approx \left[1 + \frac{2\gamma V_m}{rRT}\right] \quad (4)$$

The size-dependent solubility of the NPs is approximated by the first two elements of the Taylor series of the Gibbs–Thomson equation. Although this approximation is arguable for small sized NPs, it allows explicit expression of the size-dependent growth rate of NPs. The  $S$  value is calculated for the QOR method by using eq 4. In this equation, the  $r$  value is taken as 1 nm (corresponds to the size of SNPs) and the other values used are given in Table 1. The calculated  $S$  is used in eq 3a to calculate the growth rate of NPs for each step. The  $S$  value for the MI method is calculated by converting the corresponding number of monomers in SNPs, and as a result those two methods have the same initial number of monomers in the simulation as in the QOR method in order to compare directly the two methods. Values of  $V_m$ ,  $\gamma$ , and  $T$  used here are also given in Table 1.<sup>4</sup>

Simulation is carried out as follows (Figure 1). First, the initial size distributions are generated. The loop starts with the calculation of the growth rates for any given particle based on the  $S$  value of the solution (Figure 1, step 1). As expected, the  $S$  values are different for MI and QOR, even though the same number of monomers is present in both solutions. The initial  $S$  value of the QOR method is chosen to correspond to the  $S$  value

from the size of SNP based on eq 4. The  $S$  value of the MI method is significantly higher than that of the QOR and OR methods. This  $S$  value is the sum of  $S$  from the QOR method +  $S$  calculated from the monomers present in the SNPs. The second step in the simulation is the calculation of the new size after adding the corresponding number of monomers in each step (Figure 1, step 2). In this step, if the new size of the particle is less than zero, the particle is dissolved, resulting in a decrease in the number of particles. After calculating the new size, a new number of monomers (step 3) and the change in the supersaturation value (step 4) are calculated. In the next step, statistical parameters are calculated (step 5), such as mean radius and standard deviation, which examine the origin of the focusing in this particular growth process. Then as a last step the data are saved and the next cycle starts. A summary of the steps of this simulation is shown in Figure 1. In this simulation, the data are obtained by using specific parameters for CdSe NPs (Table 1<sup>4</sup>). The program successfully reproduced Talapin's previous work ensuring the correct implementation of the code.<sup>4</sup>

## Results and Discussion

To investigate the size focusing from QOR, many of the most relevant simulation parameters to the experiment are systematically varied, including the number of particles, initial supersaturation, and sizes of SNPs and larger NPs present in the solution. Figure 2a shows a typical size evolution of particles consisting of an initial bimodal size distribution. The data illustrate the size histogram with  $80 \times 10^3$  SNPs ( $r = 1 \text{ nm} \pm 0.1$ ) and  $2 \times 10^3$  larger NPs ( $r = 3.5 \text{ nm} \pm 0.35$ ). The black line indicates the change of critical radius over time. At the early stages of the simulation, the figure clearly shows the disappearance of SNPs that are smaller than the critical radius (eq 1). Since the radii of large particles are greater than the critical radius, they undergo growth at the expense of SNPs. Later on, as the particles grow and the supersaturation drops as well as the critical radius shifts to larger particles, the larger sized NPs will undergo Ostwald ripening, as shown by the broadening of the size distribution of larger sized NPs. At the end of the simulation, the size distribution is asymmetric and corresponds to the distribution expected from LSW theory. Figure 2b shows the typical Ostwald ripening of the nanoparticles if no SNPs are added. In addition to the Ostwald ripening, a multiple injection method is also simulated. In this case (Figure 3c), the monomer present in the SNP in Figure 2a are added as monomer creating a highly supersaturated solution with respect to the monomer. Here focusing takes place in a much shorter time scale followed by the typical Ostwald ripening at the later stage of the growth. In the next section, the statistical parameters are analyzed to carefully compare the effect of SNP on the growth of the larger sized NPs.

Figure 3 shows the temporal evolution of the statistical parameters. Simulation of the time evolution of the number of particles, size distribution, supersaturation, and average size is carried out for different methods: While the supersaturation and number of particles include all particles present in the growth solution, the size and size distribution of only the larger particles are calculated (assuming that once the reaction is over, only the larger NPs will remain and the SNPs will completely dissolve). In OR, no new particles or precursors are added to the growth solution; as a result, average size gets larger and defocusing of size distribution takes place. In QOR,  $8 \times 10^3$  small sized SNP ( $r = 1 \text{ nm} \pm 0.1$ ) of CdSe particles are added to  $2 \times 10^3$  larger size particles ( $r = 3.5 \text{ nm} \pm 0.35$ ). In the MI method, the corresponding supersaturation value of QOR is

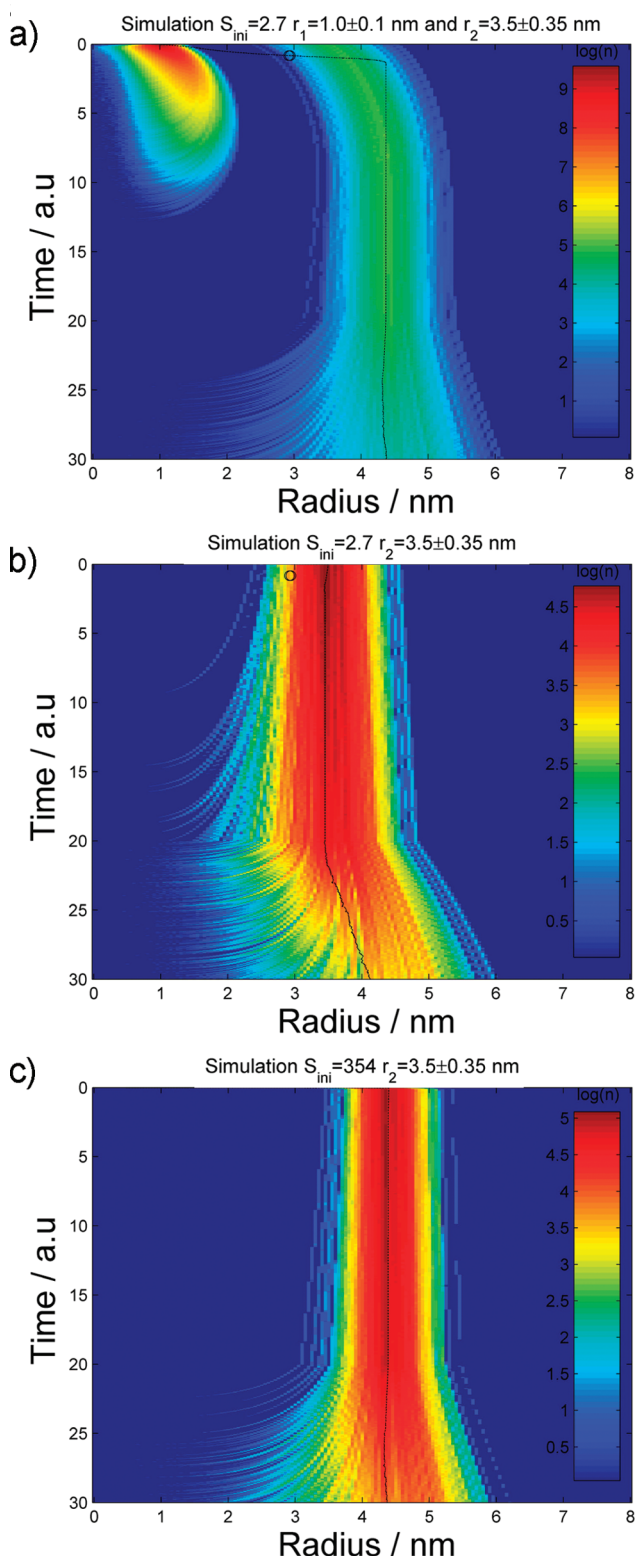


**Figure 2.** (a) Simulated temporal evolution of size histogram of  $2 \times 10^3$  NPs ( $r = 3.5$  nm  $\pm 0.35$ ) in the presence of sacrificial NP ( $80 \times 10^3$  NPs  $r = 1$  nm  $\pm 0.1$ ). The NPs undergo slow size focusing followed by defocusing when the sacrificial NPs dissolved. (b) Simulated temporal evolution of size histogram of  $2 \times 10^3$  NPs ( $r = 3.5$  nm  $\pm 0.35$ ) in the absence of sacrificial NPs. The NPs undergo Ostwald ripening. (c) Simulated temporal evolution of size histogram of  $2 \times 10^3$  NPs ( $r = 3.5$  nm  $\pm 0.35$ ) in the presence of monomers dissolved in the solution. The number of monomers is equivalent to the monomers present in the sacrificial NPs in part a. The NPs undergo rapid size focusing followed by defocusing when the sacrificial NPs dissolved. On each graph the black line shows the change of critical radius with time.

calculated (354 from eq 4) and added to the reaction solution, as in the repeated injection method.<sup>7,25</sup> In other words, while in MI the precursor and in the QOR method an equivalent amount of SNPs (sacrificial nanoparticles) is added to the solution containing a larger size. The observation is that the number of particles will decrease over time. These SNPs dissolve and, consequently, provide the monomers necessary for the larger NPs to grow. The dissolution of particles is rather slow in the case of QOR. Therefore, the growth takes longer when it is compared to the MI method. In QOR, the SNPs provide constant addition of dissolved monomers to the solution and to the larger size NPs. Therefore, the increased supersaturation from the presence of SNPs with highly curved surfaces lasts longer for QOR than in the case of MI, as shown in Figure 3. Once SNPs are consumed, the size distribution defocuses via the “regular” Ostwald ripening process.

Figure 4 summarizes the effects of different methods with the change of concentration of initial SNPs. The simulations show that the presence of a larger number of initial SNPs enhances the focusing of the larger sized (better size focusing) NPs. It is speculated that the limit of these experiments will be based on the solubility of the SNPs in the solutions. Although the MI method creates a faster and somewhat tighter focusing than QOR, it is harder to control the growth of NPs experimentally. On the other hand, QOR’s slow size focusing is advantageous to control the overall growth of the NPs in the solution. Potentially, the slower growth also may yield better quality nanocrystals if the defect removal rate is slower than the growth in the case of the MI method. Finally, Figure 5 shows the effect of increasing concentration of the SNPs on the supersaturation of QOR. When dissolution of particles takes place, the supersaturation of the larger number of particles tends to increase faster than the others. All of the different supersaturation values reach a similar maximum value and behave the same way at the latter stage of the NP growth.

Previously, a set of fixed-sized particles have been simulated to explore the effect of varying the number of particles on average size, supersaturation, size distribution, and number of particles. Simulations of changing the sizes of larger particles are carried out to investigate the effect on focusing. The results are summarized in Figure 6. The total number of particles in the solution shows a slow decreasing pattern with decreasing size. This is caused by the close size of the SNPs to the critical size. A plot of the size distribution (Figure 6) illustrates how the size distribution is changing with respect to time. A general pattern of lower size distribution is seen toward the smaller sizes. A sudden drastic increase in QOR is observed for 3 nm particles, which originates from the small difference in the two sizes present. This is an artifact that is the result of the overlapping size distributions. Although numerically this artifact can be removed by labeling the NPs to specify where distributions are originated from, this indicates the lower limit of how close the size distributions can be placed without interference. A decrease of size results in a slower decrease in supersaturation values, which can be expected on the basis of the decreases of overall surface area of the larger size NPs. The graph also shows that larger size results in larger average size. Small particles dissolve faster and help the larger size grow.

When focusing of NPs takes place, the standard deviation of the NPs gets smaller. A high initial particle (monomer) concentration, as Talapin’s work pointed out,<sup>4</sup> yields fast focusing of size distribution. Therefore, as higher supersaturation values are implemented, the focusing takes place faster and smaller NP size distributions are obtained. In bimodal size

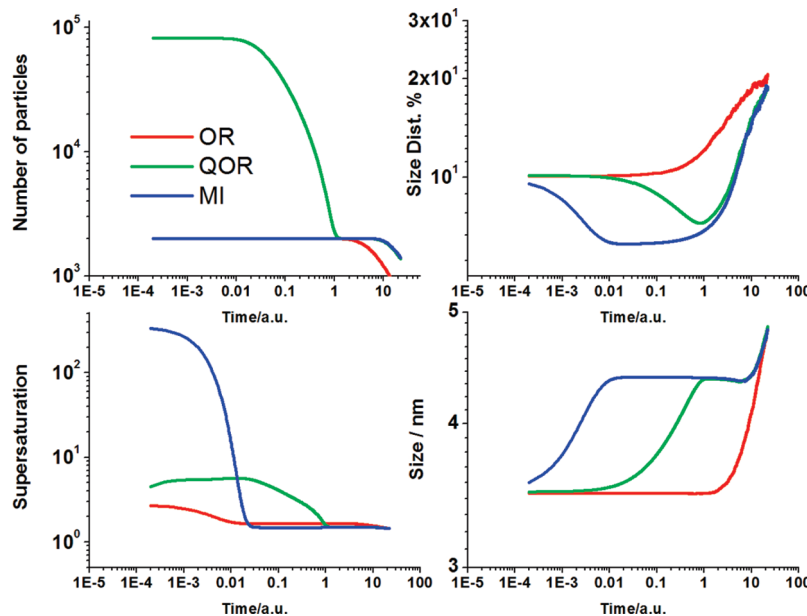


**Figure 3.** Simulation of the time evolution of number of particles, size distribution, supersaturation, and size for different methods: OR (Ostwald Ripening) is shown by red lines, QOR (quantized Ostwald ripening) is green lines, MI (multiple injection) is blue lines.

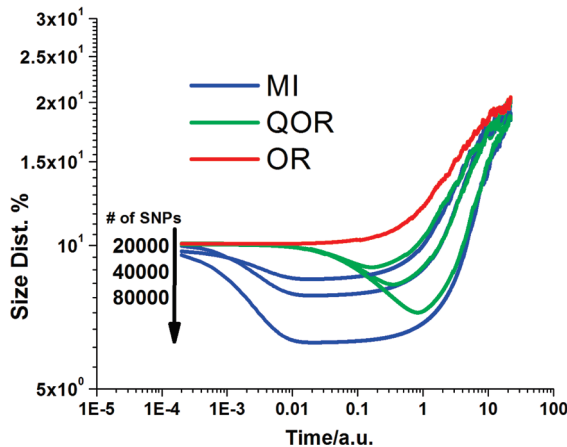


**Figure 4.** Temporal change of size distribution for MI, QOR, and OR with addition of different numbers of SNPs.

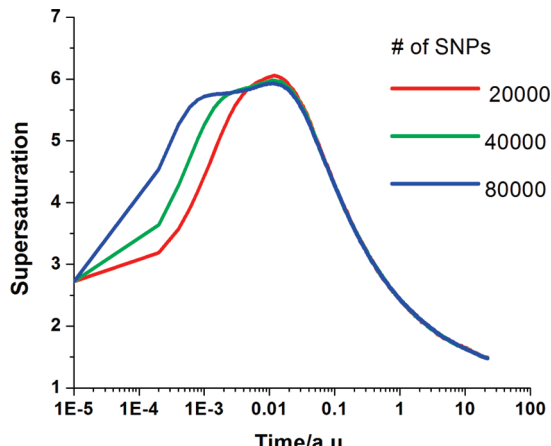


**Figure 5.** Temporal change of supersaturation with different initial number of small particles (first size).

distribution, since there are two different sizes, the effect of higher initial number of particles on the size distribution is explored. The simulations are carried out by changing the concentration of SNPs and large sizes independently. Figure 7

left shows the change of standard deviation with respect to the number of SNPs while the number of larger size nanoparticles is kept constant. The number of SNPs is varied between 0 and 1.6 × 10<sup>5</sup>. As a larger number of initial particles is used, the standard deviation of the larger size gets smaller; therefore, better size focusing is achieved. As more monomers are being produced, they will provide the necessary material to the growth of the larger particles. In the next simulation (Figure 7 right), the number of SNPs is kept constant (8 × 10<sup>4</sup>) and the number of large sized nanoparticles is varied from 5 × 10<sup>2</sup> to 8 × 10<sup>3</sup>. In this case, as the concentration of the larger NPs increases, the size distribution of the larger NPs reaches a minimum followed by a further increase. To summarize this figure, when the increase of the concentration of SNPs is advantageous to achieve better focusing, the concentration increase of the larger size NPs affects the focusing in a reverse way.

In hot injection techniques, the precursors are injected rapidly to growth solution in a typical synthesis<sup>17,26,27</sup> to separate nucleation and growth.<sup>17,26,27</sup> In order to examine and compare the renucleation rates in this system, renucleation rates of the multiple injection method to the quantized Ostwald ripening has been calculated given by the following equations:<sup>4</sup>

$$J_N = B_N \exp\left(-\frac{\Delta G_N}{RT}\right) \quad (5)$$

$$\Delta G_N = \frac{16\pi\gamma^3 V_m^2}{3(RT \ln S)^2} \quad (6)$$

In these equations,  $\Delta G_N$  is the activation energy of homogeneous nucleation,  $B_N$  represents pre-exponential factor, and  $J_N$  gives the rate of nucleation. When QOR and MI are compared, the renucleation rate is almost 10<sup>4</sup>-fold higher for MI (Figure 8). The large difference in the renucleation rate in these two methods is mainly because of the very different  $S$  values. Thus, the QOR technique could yield much lower renucleation and, therefore, less polydispersity in the NP solution. The dependence of renucleation rates on the SNP

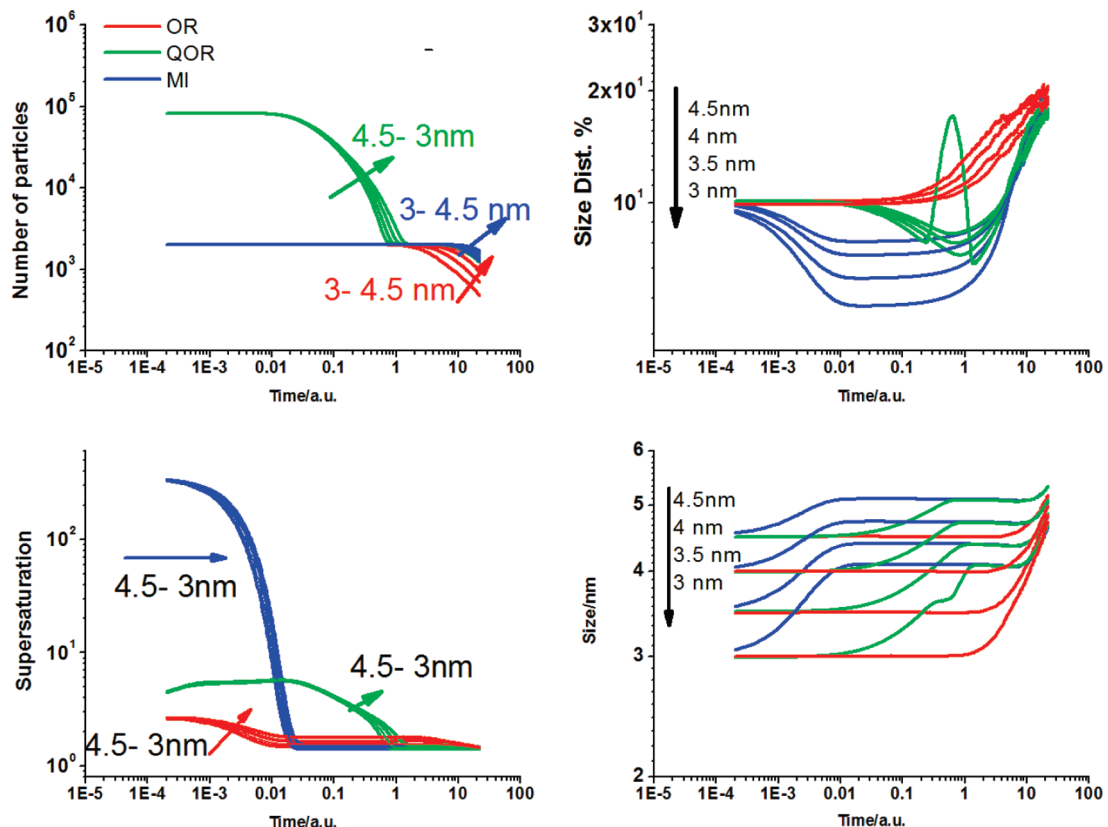


**Figure 6.** Temporal evolutions of the number of particles, size distribution, supersaturation, and size values are shown for different initial sized larger particles. The arrows show the direction of the size change for corresponding sizes (3–4.5 nm).

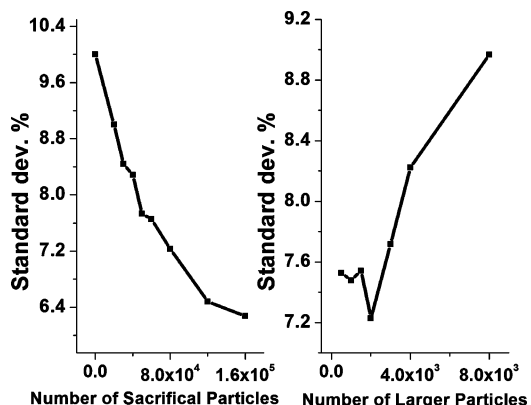


**Figure 7.** Change of standard deviation with addition of different number of particles: (left) SNPs and (right) larger sized nanoparticles.

concentration is also shown in the figure. The larger number of initial particles results in higher renucleation rates. As noted earlier, a limit of the applicability of this approach is the solubility of the SNPs in the solution. In order to compare the solubility of NPs used in the simulation to the experimental data, volume fractions of NPs under the experimental conditions are calculated. All the calculated results from the synthetic data show that solubility used in the simulation is below the solubility limit of typical CdSe NPs in the growth solution. For example, the volume fractions of the NPs in the literature are found to be  $0.34 \times 10^{-3}$  (radius of the NPs is 1 nm),<sup>28</sup>  $1.13 \times 10^{-3}$  (radius of the NPs is 0.8 nm),<sup>29</sup> and  $2.70 \times 10^{-3}$  (radius of the NPs is 0.75 nm),<sup>30</sup> and the volume fraction used in the simulation is below  $10^{-3}$ . This also means that possible diffusional interactions between the neighboring particles can be ignored. As expected, the simulation will be sensitive to the

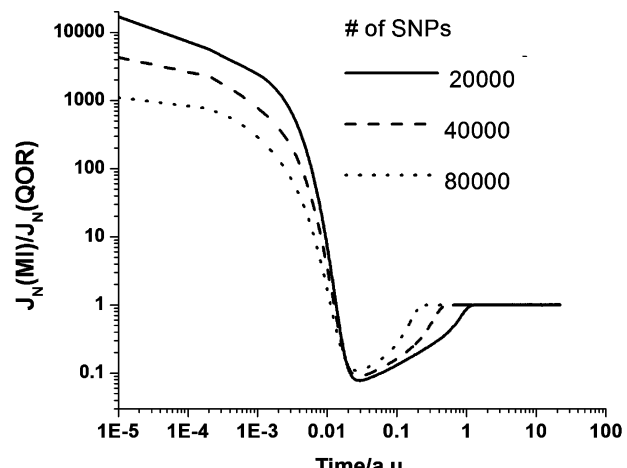


**Figure 8.** Comparison of rate of renucleation of MI to the QOR with different initial number of sacrificial particles added.

surface energy of the particles. The increase in surface energy will result in a faster kinetics and shifts the location of the critical radius. Besides, the specific surface energy value that is used in the overall simulation ( $0.125 \text{ J/m}^2$ ), two different values, 0.15 and  $0.1 \text{ J/m}^2$ , are also implemented into the simulation to investigate the effect of surface energy on the kinetics. The behavior of growth solution is similar to the presented one. The only difference is that, with the larger surface energy, faster overall growth is observed.

## Conclusions

In summary, a kinetic simulation of NPs has been carried out to explore the size evolution of the bimodal distribution of NPs. The results show the focusing of size distribution after

the addition of smaller SNP below the critical radius as a result of Ostwald ripening (large particles grow on the expense of the small particles). In this quantized Ostwald ripening, smaller sized particles from a bimodal size distribution of particles dissolve and larger ones grow similarly to the regular Ostwald ripening which results in focusing of size distribution of larger particles. A key goal in NP synthesis is producing high-quality NPs with very narrow size distribution. This has already been achieved by multiple injection techniques experimentally.<sup>7</sup> The difference between multiple-injection and this proposed method is the time required to achieve size focusing. Under the same monomer concentration, the quantized Ostwald ripening method extends the time required for the focusing compared to the multiple injection method. Therefore, this slower growth allows an easier scaling up of the NP synthesis than in the multiple injection method due to its less susceptibility to circumstances when heat and mass transfer are limited. In addition, the QOR method reduces the occurrence of the renucleation process observed mostly in the multiple injection method. It is anticipated that the proposed method can be extended to design nanoparticle growth solutions that are self-focusing (no multiple injection is needed) to enrich a desired size distribution function with controllable focusing times. This would require the mixing of particles with arbitrary size distributions.

**Acknowledgment.** The authors would like to acknowledge Kansas State University and the Department of Chemistry for the support of this research. This work was supported by ACS under contract ACS PRF #49320-DNI10.

## References and Notes

- (1) Marqusee, J. A.; Ross, J. Kinetics of Phase-Transitions—Theory of Ostwald Ripening. *J. Chem. Phys.* **1983**, *79* (1), 373–378.
- (2) Oriani, R. A. Ostwald Ripening of Precipitates in Solid Matrices. *Acta Metall.* **1964**, *12* (12), 1399.
- (3) Marqusee, J. A.; Ross, J. Theory of Ostwald Ripening—Competitive Growth and Its Dependence on Volume Fraction. *J. Chem. Phys.* **1984**, *80* (1), 536–543.
- (4) Talapin, D. V.; Rogach, A. L.; Haase, M.; Weller, H. Evolution of an Ensemble of Nanoparticles in a Colloidal Solution: Theoretical Study. *J. Phys. Chem. B* **2001**, *105* (49), 12278–12285.
- (5) Voorhees, P. W. The Theory of Ostwald Ripening. *J. Stat. Phys.* **1985**, *38* (1–2), 231–252.
- (6) Tonti, D.; Mohammed, M. B.; Al-Salman, A.; Pattison, P.; Chergui, M. Multimodal Distribution of Quantum Confinement in Ripened CdSe Nanocrystals. *Chem. Mater.* **2008**, *20* (4), 1331–1339.
- (7) Peng, X. G.; Wickham, J.; Alivisatos, A. P. Kinetics of II-VI and III-V Colloidal Semiconductor Nanocrystal Growth: “Focusing” of Size Distributions. *J. Am. Chem. Soc.* **1998**, *120* (21), 5343–5344.
- (8) Yao, J. H.; Elder, K. R.; Guo, H.; Grant, M. Theory and Simulation of Ostwald Ripening. *Phys. Rev. B* **1993**, *47* (21), 14110–14125.
- (9) De Smet, Y.; Deriemaeker, L.; Finsy, R. A Simple Computer Simulation of Ostwald Ripening. *Langmuir* **1997**, *13* (26), 6884–6888.
- (10) Qu, L. H.; Peng, Z. A.; Peng, X. G. Alternative Routes toward High Quality CdSe Nanocrystals. *Nano Lett.* **2001**, *1* (6), 333–337.
- (11) Dabbousi, B. O.; RodriguezViejo, J.; Mikulec, F. V.; Heine, J. R.; Mattoussi, H.; Ober, R.; Jensen, K. F.; Bawendi, M. G. (CdSe)ZnS Core-Shell Quantum Dots: Synthesis and Characterization of a Size Series of Highly Luminescent Nanocrystallites. *J. Phys. Chem. B* **1997**, *101* (46), 9463–9475.
- (12) Vossmeyer, T.; Katsikas, L.; Giersig, M.; Popovic, I. G.; Diesner, K.; Chemseddine, A.; Eychmuller, A.; Weller, H. CdS Nanoclusters—Synthesis, Characterization, Size-Dependent Oscillator Strength, Temperature Shift of the Excitonic-Transition Energy, and Reversible Absorbency Shift. *J. Phys. Chem.* **1994**, *98* (31), 7665–7673.
- (13) Katari, J. E. B.; Colvin, V. L.; Alivisatos, A. P. X-ray Photoelectron-Spectroscopy of CdSe Nanocrystals with Applications to Studies of the Nanocrystal Surface. *J. Phys. Chem.* **1994**, *98* (15), 4109–4117.
- (14) Reiss, H. The Growth of Uniform Colloidal Dispersions. *J. Chem. Phys.* **1951**, *19* (4), 482–487.
- (15) Battaglia, D.; Peng, X. Formation of High Quality InP and InAs Nanocrystals in a Noncoordinating Solvent. *Nano Lett.* **2002**, *2* (9), 1027–1030.
- (16) Yang, Y. A.; Wu, H. M.; Williams, K. R.; Cao, Y. C. Synthesis of CdSe and CdTe nanocrystals without precursor injection. *Angew. Chem.-Int. Ed.* **2005**, *44* (41), 6712–6715.
- (17) Murray, C. B.; Norris, D. J.; Bawendi, M. G. Synthesis and Characterization of Nearly Monodisperse CdE (E = S, Se, Te) Semiconducting Nanocrystallites. *J. Am. Chem. Soc.* **1993**, *115* (19), 8706–8715.
- (18) Wang, H. L.; Ning, D.; Feng, S. L. Temperature Dependence of the Optical Properties of InAs/GaAs Self-Organized Quantum Dots with Bimodal Size Distribution. *J. Cryst. Growth* **2000**, *209* (4), 630–636.
- (19) Zhao, H. G.; Chaker, M.; Ma, D. L. Bimodal Photoluminescence during the Growth of PbS Quantum Dots. *J. Phys. Chem. C* **2009**, *113* (16), 6497–6504.
- (20) Tuinenga, C.; Jasinski, J.; Iwamoto, T.; Chikan, V. In Situ Observation of Heterogeneous Growth of CdSe Quantum Dots: Effect of Indium Doping on the Growth Kinetics. *Acad. Nano* **2008**, *2* (7), 1411–1421.
- (21) Fu, M.; Hu, Z. S.; Tang, M.; Wei, X. P.; Shao, M. H.; Li, L. H.; Deng, Y. L. Supersaturation Control Growth of Nanoparticle ZnO and Size Distribution Control. *Chinese J. Chem. Phys.* **2007**, *20* (6), 811–815.
- (22) Thessing, J.; Qian, J. H.; Chen, H. Y.; Pradhan, N.; Peng, X. G. Interparticle Influence on Size/Size Distribution Evolution of Nanocrystals. *J. Am. Chem. Soc.* **2007**, *129* (10), 2736.
- (23) Ross, F. M.; Tersoff, J.; Tromp, R. M. Coarsening of Self-Assembled Ge Quantum Dots on Si(001). *Phys. Rev. Lett.* **1998**, *80* (5), 984.
- (24) He, R.; You, X.; Tian, H.; Gao, F.; Cui, D.; Gu, H. Synthesis and Characterization of Monodisperse CdSe Quantum Dots in Different Organic Solvents. *Frontiers Chem. China* **2006**, *1* (4), 378–383.
- (25) Peng, X. G.; Manna, L.; Yang, W. D.; Wickham, J.; Scher, E.; Kadavanich, A.; Alivisatos, A. P. Shape Control of CdSe Nanocrystals. *Nature* **2000**, *404* (6773), 59–61.
- (26) Li, L.; Reiss, P. One-Pot Synthesis of Highly Luminescent InP/ZnS Nanocrystals without Precursor Injection. *J. Am. Chem. Soc.* **2008**, *130* (35), 11588.
- (27) Donega, C. D.; Liljeroth, P.; Vanmaekelbergh, D. Physicochemical Evaluation of the Hot-Injection Method, A Synthesis Route for Monodisperse Nanocrystals. *Small* **2005**, *1* (12), 1152–1162.
- (28) Peng, Z. A.; Peng, X. G. Nearly Monodisperse and Shape-Controlled CdSe Nanocrystals via Alternative Routes: Nucleation and Growth. *J. Am. Chem. Soc.* **2002**, *124* (13), 3343–3353.
- (29) Riehle, F. S.; Bienert, R.; Thomann, R.; Urban, G. A.; Krugert, M. Blue Luminescence and Superstructures from Magic Size Clusters of CdSe. *Nano Lett.* **2009**, *9* (2), 514–518.
- (30) Bowers, M. J.; McBride, J. R.; Rosenthal, S. J. White-Light Emission from Magic-Sized Cadmium Selenide Nanocrystals. *J. Am. Chem. Soc.* **2005**, *127* (44), 15378–15379.